HHS Public Access

Author manuscript

Magn Reson Imaging. Author manuscript; available in PMC 2014 April 14.

Published in final edited form as:

Magn Reson Imaging. 2013 April ; 31(3): 385–395. doi:10.1016/j.mri.2012.08.010.

Image domain propeller fast spin echo☆

Stefan Skare[a,b], **Samantha J. Holdsworth**[c], **Anders Lilja**[a,b], and **Roland Bammer**[c]

[a]Clinical Neuroscience, Karolinska Institutet, Stockholm, Sweden

[b]Department of Neuroradiology, Karolinska University Hospital, Stockholm, Sweden

[c]Center of Quantitative Neuroimaging, Department of Radiology, Stanford University, Stanford, CA, USA

Abstract

A new pulse sequence for high-resolution T2-weighted (T2-w) imaging is proposed –image domain propeller fast spin echo (iProp-FSE). Similar to the T2-w PROPELLER sequence, iProp-FSE acquires data in a segmented fashion, as blades that are acquired in multiple TRs. However, the iProp-FSE blades are formed in the image domain instead of in the *k*-space domain. Each iProp-FSE blade resembles a single-shot fast spin echo (SSFSE) sequence with a very narrow phase-encoding field of view (FOV), after which *N* rotated blade replicas yield the final full circular FOV. Our method of combining the image domain blade data to a full FOV image is detailed, and optimal choices of phase-encoding FOVs and receiver bandwidths were evaluated on phantom and volunteers. The results suggest that a phase FOV of 15–20%, a receiver bandwidth of ±32–63 kHz and a subsequent readout time of about 300 ms provide a good tradeoff between signal-to-noise ratio (SNR) efficiency and T2 blurring. Comparisons between iProp-FSE, Cartesian FSE and PROPELLER were made on single-slice axial brain data, showing similar T2-w tissue contrast and SNR with great anatomical conspicuity at similar scan times –without colored noise or streaks from motion. A new slice interleaving order is also proposed to improve the multislice capabilities of iProp-FSE.

Keywords

MRI; Propeller; T2-w; Pulse sequences; Reduced FOV

1. Introduction

For nearly all patients undergoing MRI today, high-resolution T2-weighted (T2-w) imaging plays a key role in the examination. For T2-w image contrast, the fast spin-echo (FSE) sequence [1] is typically used due to its good contrast and SNR efficiency –with image artifacts mostly limited to image ghosting caused by patient motion.

☆This work was supported in part by the Swedish Research Council (K2007-53P- 20322-01-4), the NIH (5R01EB002711, 1R21EB006860, 1R01EB008706 and 1R01EB006526, the Center of Advanced MR Technology at Stanford (P41RR09784), the Oak Foundation, GE Healthcare and the Lucas Foundation.

*Corresponding author. stefan@skare.se (S. Skare).

To avoid image ghosting due to head motion, the T2-w PROPELLER pulse sequence [2,3] has been implemented as an alternative to FSE and is currently available on most commercial MR systems. In PROPELLER, the RF-refocused echoes in the readout train are placed as a rectangular strip, or blade, over the center of *k*-space with the 'length' of the blade along the frequency-encoding direction. The remaining areas of *k*-space are acquired in subsequent TRs by rotated replicas of the *k*-space blade trajectory (hence, the acronym PROPELLER). With its centrally overlapping blades, PROPELLER is a self–navigated technique, allowing for both image domain phase correction (that centers and focuses the blades in *k*-space) as well as in-plane (2D) motion correction between the blades. Because all blades cover the center of *k*-space, a noise-suppressing averaging effect results for low spatial frequencies, and the remaining high-frequency noise may render the image somewhat 'speckled' if the overall SNR is limited.

In this article, we present a new pulse sequence, *i*mage domain *Prop*eller *FSE* (iProp-FSE), where data are collected in a similar propeller fashion to PROPELLER, but where the blades are formed and stitched together in the image domain. While each *k*-space PROPELLER blade constitutes a full FOV image at low resolution along the phase-encoding direction (Fig. 1A), an iProp-FSE blade covers a narrow strip of the image FOV at *full* image resolution (Fig. 1B), with the phase-encoding FOV (FOV_{phase}) and frequency-encoding FOV (FOV_{freq}) along the short and long axes, respectively. Subsequent blades are rotated around the center of the image FOV to cover the rest of the missing anatomy. The blade overlap that occurs at the center of the image FOV effectively produces a local averaging effect (NEX) corresponding to N_{blades}. For regular head exams, the center of the FOV is typically the most SNR-starved area, as it usually coincides with the location that is furthest away from the coil elements. For example, the SNR at the brain's cortex near the coil elements may be about three to five times higher than that at the brain stem for a 32-channel head coil (Fig. 3A). With overlapping image domain blades, the low SNR at the center of the coil is compensated for by more local averages centrally, which helps to even out the SNR over the entire brain.

However, to make the iProp-FSE to work in practice, the first step is to overcome the aliasing of anatomy located outside the narrow blade FOV along each blade's phase-encoding direction. Previous work (in the context of diffusion imaging), including zonally magnified (ZOOM) EPI [4], contiguous slice zoom EPI [5] and reduced FOV techniques for spine imaging [6], has, in various ways, shown how a rectangular image FOV can be obtained without aliasing. Common for these methods is that the excitation and refocusing slice planes are played out at an angle relative to each other to avoid signal outside the intended FOV. For iProp-FSE, we have chosen to avoid aliasing outside the phase-encoding FOV by tilting the excitation pulse by a relatively low tilt angle, with the train of refocusing pulses played out in the prescribed image plane.

Deng and Larson [7] have recently proposed a related T2-w PROPELLER technique using an out-of-plane excitation, dubbed *targeted PROPELLER MRI*, where only a part of the anatomy is shown in the final image. In Ref. [7], standard *k*-space gridding was performed with the final image corresponding to the intersecting area of the iProp-FSE blades presented in this work.

The main objectives of this initial study on iProp-FSE were to investigate

1. how the iProp blades are to be combined seamlessly in the image domain (weighted image-domain gridding).
2. how the effective resolution and SNR are affected by the echo train length, controlled by the choice of receiver bandwidth and the blade width (FOV_{phase}) for a given target resolution.
3. the amount of reduction in SNR and image contrast for contiguous multislice iProp-FSE imaging due to the out-of-slice saturation effect from the tilted slices.
4. whether iProp-FSE can yield a high-resolution T2-w image contrast with a SNR efficiency similar to the commercially available FSE and PROPELLER sequences.

2. Methods

2.1. Data acquisition

The iProp-FSE sequence is, in many ways, similar to the single-shot fast spin-echo (SSFSE) pulse sequence [8,9], but with a significantly reduced FOV_{phase}, with N_{blades} dynamically rotated replicas of the prescribed FOV and with an extra gradient added along the phase-encoding direction during the excitation (Fig. 2A). With a linear combination of the two slice selective excitation gradient amplitudes, the resulting excitation slab is played out at a given angle in the slice/ phase-encoding plane, with a slab thickness that was automatically adjusted based on the prescribed FOV_{phase} (Fig. 2B and C). Due to the tilted excitation plane, only spins experiencing both the excitation and the refocusing pulses contribute to the MR signal (green area, Fig. 2B and C). For any excitation tilt angle below 90°, the slice thickness will consequently approach zero at the edges of the phase FOV. This slice narrowing effect is more pronounced for lower tilt angles and for lower FOV_{phase} (Fig. 2B and C). The slice thickness of the resulting ‘rhomboid’ will, in practice, also be further smoothed due to the nonrectangular slice profiles of the RF pulses themselves.

At each TR, a rotation matrix was applied to the logical gradient coordinate system to effectively rotate the rectangularly shaped FOV within the prescribed image plane. As this rotation simply corresponds to a given linear combination of the physical gradients, which have a common origin at the isocenter of the bore of the magnet, this also affects in-plane translations of the FOV. Hence, for an oblique image plane or an off-centered FOV, adjustments of the receiver phase and frequencies, unique for each blade, were necessary to make the image domain blades rotate around the prescribed image center. Similarly, the frequency of the RF pulse for the tilted excitation was also adjusted for each blade angle to excite the proper tilted slab location for any arbitrary image plane and FOV offset.

With an excitation tilt angle of 30°, all but one experiment were performed in single-slice mode to exclude saturation (or crosstalk) effects from the tilted excitation slab onto neighboring slices. For one multislice experiment, a second tilt angle of 15° was also attempted to investigate crosstalk effects. The rationale for this can be seen by the size of the gray wedges in Fig. 2B and C, where a reduced tilt angle also implies that fewer neighboring slices are hit by the tilted excitation slab. With only approximately 100 ms between two

consecutively acquired slices, a significant reduction in longitudinal magnetization will therefore occur if the next-coming slice is placed inside this area.

The refocusing pulses were 1.2 ms in duration, allowing for a short echo spacing from 5.8 to 10.4 ms for the receiver bandwidths (rBW=±32, ±63 kHz) and frequency-encoding resolutions (N_{freq}= 320, 448) used in this work. Similar to many SSFSE acquisitions, half-Fourier encoding was used in the phase-encoding direction to reduce the echo train length. Refocusing flip angles of 155° were used to limit the RF heating (Specific Absorption Rate [SAR]). The number of 'overscans' (i.e., extra phase-encoding lines beyond half of *k*-space) was adjusted to between 6 and 13 (depending on other scan parameters) to maintain an effective TE of around 80 ms (78–87 ms). The number of blades used was adjusted with the chosen FOV_{phase} to fill the entire circular image FOV.

iProp-FSE data were acquired on both phantoms and humans using a GE 3-T Discovery MR750 system equipped with a 50 mT/m, SR=200 T/(m s) gradient set (GE Healthcare, Waukesha, WI, USA). A 32-channel RF coil (MRI Instruments, Inc., Minneapolis, MN, USA) was used throughout the study. Single slice, fat-saturated, iProp-FSE data were acquired with a 320×320 image resolution, 4 mm slice thickness and a FOV of 22 cm, unless stated otherwise below. All human scans were approved by the local ethics committee. Specifically, the following experiments were conducted:

1. Two-dimensional axial relative SNR maps, $C(x,y)$, were calculated for two multi-channel receive-only RF coils; an eight-channel head coil (InVivo Corporation, Florida, USA) and the above-mentioned 32-channel coil. An axial slice of a spherical phantom (18 cm) using a GRE sequence with 100 repetitions was used for this purpose (FOV=22 cm, TE/TR= 3.3/7.4 ms, 256×256). At each pixel location, $C(x,y)$ was calculated by taking the ratio of the mean and the standard deviation across repetitions. Sampling density maps, $D(x,y)$, from ideal iProp-FSE blades with FOV_{phase}/FOV_{freq} ratios of 0.1, 0.15, 0.20 and 0.26 were calculated by gridding 1's using a minimal set of blades for each FOV_{phase}. As the sampling density map also shows the number of averages at each spatial location, the square root of the sampling density should correspond to the local SNR due to this averaging. Therefore, accounting for both the data sampling pattern and the particular coil used, the final SNR was calculated via the product $S(x,y)=C(x,y)\sqrt{D(x,y)}$.

2. Measurements of effective resolution with iProp-FSE vs. FOV ratio (0.10-0.26) and rBW (±32, ±63 kHz) were performed on the vendor's daily quality assurance phantom containing plastic resolution structures surrounded by doped water. This phantom had a T2 and T1 of 80 and 150 ms, respectively. With the T2 value being close to that of the brain white matter (WM) and gray matter (GM), the effective resolution measurements (subject to T2 blurring) should translate fairly well to the brain. The TE/TR was 52/500 ms for these measurements, which is lower than for corresponding in vivo scans, but neither TE nor TR should affect the level of T2 blurring. Conventional SSFSE data with rBW of ±83 kHz were also acquired for

comparison, along with a 512×512 classical spin-echo image for geometrical reference.

3. An axial slice of a healthy volunteer was acquired using the same scan parameters as for the effective resolution experiment (except here TE/TR=~80/4000 ms). For each combination of FOV_{phase} and rBW, two consecutive scans were acquired to generate a SNR map, $S(x,y)$, of the final image. To increase the statistical power, two regions of interest (ROIs) were placed on the SNR maps, one within the region where the blades overlap and another one laterally of this region. In addition to the relative SNR measurements, the images were visually compared in an attempt to find which range of phase FOVs and rBWs demonstrates the best trade-off between sharpness, tissue contrast and noise. Moreover, a relative SNR efficiency metric was calculated for the off-center ROI for single- and multislice scan scenarios (assuming no cross-talk problems) according to the following equations (long TR limit, without T1 effects):

$$\eta_{\text{singleslice}} = \frac{\text{SNR}_{\text{ROI}}}{\sqrt{N_{\text{blades}}}} \quad (1)$$

for the single-slice case, and

$$\eta_{\text{multislice}} = \frac{\text{SNR}_{\text{ROI}}}{\sqrt{T_{\text{seq}} N_{\text{blades}}}} \quad (2)$$

for the multislice case, assuming a maximum number of slices per TR, and where T_{seq} in Eq. (2) stands for the pulse sequence length (from the first fat-saturation pulse to the last spoiler gradient).

4. The effect of cross-talk in multislice imaging caused by the tilted excitation slab in iProp-FSE was investigated by scanning the axial slices of a volunteer's brain, in the following three acquisition modes:

   a. single slice (no cross-talk). TR=10 s.

   b. standard interleaved multislice with 32 slices, covering 12.8 cm of the brain in the superior–inferior direction (minimum TR=13 s), with the slices acquired in the following temporal order (odd slices first, followed by even slices): 1-3-5-7-9-11-13-15-17-19-21-23-25-27-29-31–2-4-6-8-10-12-14-16-18-20-22-24-26-28-30-32.

   c. same as in (b) but with a new ‘double-interleaved–slice ordering scheme proposed here. For 32 slices, the temporal slice order using this proposed scheme becomes1-5-9-13- 17-21-25-29–3-7-11-15-19-23-27-31–2-6-10-14-18-22- 26-30–4-8-12-16-20-24-28-32. In (b), there is only one slice skip between slices acquired consecutively in time, whereas with this new slice ordering scheme, any two slices acquired after each other are separated by three full slices, or in this case a 3×4 mm=12 mm gap. We hypothesize that this will reduce the cross-talk (see Fig. 2B and C, gray

areas). For all three scan modes, data were acquired twice, using tilt angles of 15° and 30°. Lower tilt angles imply less cross-talk, but also less overlapping area between the excitation and the refocusing planes (green areas) resulting in a diminished effective slice thickness (especially at the short-axis edges of the blade FOV). For this experiment, the rBW and the FOV ratio were fixed at ±50 kHz and 0.175, respectively.

5. High-resolution brain scans using iProp-FSE, as well as the vendor's FSE, SSFSE and PROPELLER sequences, were performed on a healthy volunteer with an in-plane resolution of 448×448. For iProp-FSE and PROPELLER, the rBW was ±63 kHz, and for FSE it was set to the commonly used value of ± 31.2 kHz. The echo train length was 16, 22 and 52 for FSE, PROPELLER and iProp-FSE, respectively. Sixty blades with a FOV ratio of 0.1875 were used for iProp-FSE. Four image reconstructions were performed on the iProp-FSE data, using every sixth, third, second, and every blade, simulating iProp- FSE scans of 0:40, 1:20, 2:00 and 4:00 min in duration. Two PROPELLER scans were performed with 1.5 and 3 NEX, with scan times of 2:08 and 4:16 min, respectively. The Cartesian FSE scan was acquired in 2:00 min. The SSFSE scan was acquired in a single TR using an rBW of ±83 kHz.

6. A high-resolution iProp-FSE scan was performed on a patient with a relapsing ependymoma in the brain stem along with the patient's clinical scan. The same parameters as for the high-resolution volunteer scan above were used, except that the FOV in this case was 24 cm to match the other clinical scans. Five reconstructions were performed using every 15th (i.e., 4 blades), 10th (6 blades), 6th (10 blades), 3rd (20 blades) and all 60 blades, simulating scan times from 0:16 to 4:00 min.

2.2. Image reconstruction

For non-Cartesian imaging, including previously described *k*-space propeller sequences (PROPELLER [2], Turbo-Prop [10], SAP-EPI [11], etc.), each *k*-space sample point is equally important in the gridding process, not counting the weighting of each sample point due to its distance to the surrounding Cartesian grid points. However, near the blade edges in the short-axis direction of an iProp-FSE scan, the signal will fall off due to the tilted excitation slab (Fig. 2, green area); thus these sample points contain less signal. These data points should therefore be given reduced importance. For these locations, the data samples can be used from other iProp blades that cover the same anatomical location with greater fidelity. Hence, two problems need to be addressed.

First, the short-axis signal weighting profile, $W(p)$, needs to be determined (p denotes the phase-encoding direction). This profile will be dependent on the chosen tilt angle, FOV_{phase}, and the time-bandwidth products and effective slice thicknesses of the excitation and refocusing pulses. With these many dependencies, it may be difficult to find a general expression or lookup table to be used in the image reconstruction. One option could therefore be to measure $W(p)$ by scanning a homogeneous phantom using the same acquisition parameters as the subsequent human scan, but this is quite impractical in a

clinical routine. Instead, an estimate of $W(p)$ (assumed not to vary across blades or slices) was calculated from the acquired data itself. To reduce the effects of the tissue signal and coil sensitivities, each line in the phase-encoding direction (i.e., along the short axis of the image blade) was first normalized independently by its mean value. The weighting profile, $W(p)$, was thereafter approximated by simply averaging all normalized phase-encoding lines from all blades and slices, excluding lines with too low a mean signal. An example of the resulting profile is shown in Fig. 4D (black dashed line). Note that mainly due to some residual foldover aliasing in the phase-encoding direction, the signal profile does not quite go down to zero at the edges.

Second, with an estimate of $W(p)$, the acquired data were processed in the following manner:

1. As the blade raw data were acquired in a partial Fourier fashion, partial Fourier reconstruction using Projection Onto Convex Sets (POCS) [12,13] was first performed in *k*-space, followed by sum-of-squares averaging across coil elements in the image domain, resulting in magnitude blade image data.
2. To ensure a zero weighting of the data along the edges, a 1D Fermi filter, $F(p)$, (Fig. 4D, red dotted line) was applied to both the image domain blade data, $I(f,p,b)$, and the weighting profile, $W(p)$ (Fig. 4D, blue solid line), yielding $I_F(f,p,b)$ and $W_F(p)$, where f and p denote the frequency- and phase- encoding directions, respectively, while b indicates the blade index. The parameters for the 1D Fermi filter $F(p)$ were set to have a dominant flat response with a transition width that was empirically adjusted to suppress the edge noise and aliasing. In Matlab (The MathWorks, Natick, MA, USA) notation, the discrete 1D filter $F(b)$ is given by: F=[fliplr(f)f], where f= 1.0/{1+exp[linspace(−20,0, N_{pe}/2)]} and N_{pe} denotes the number of phase-encoding lines.
3. The N_{blades} propeller blade images were gridded separately using a standard gridding algorithm with a Kaisser–Bessel kernel. Gridding only one blade at a time essentially resembles a rotation of the image blade with zeroes padded in a common Cartesian image frame for all blades.
4. The same gridding procedure was performed for the $W_F(p)$ profile after expansion in the frequency-encoding direction to cover the same area as the image domain blade.
5. The final image was obtained by taking the ratio between the sum of squares of the gridded blades, $I_{F,grid}(x,y,b)$, and the sum of squares of the gridded weighting profiles, $W_{F,grid}(x,y,b)$, according to:

$$I(x,y)=\sqrt{\frac{\sum_{b=1}^{N_{blade}}\left(I_{F,grid}(x,y,b)\right)^2}{\sum_{b=1}^{N_{blade}}\left(W_{F,grid}(x,y,b)\right)^2}} \quad (3)$$

This procedure removes the weighting due to $W(p)$ from the data, initially imprinted across the image domain blade during acquisition, with the sum-of-squares weighted combination of the blades giving rise to a strong suppression of the low-signal areas at the edges of each blade.

6. As a final step, the signal intensity variation from the coil sensitivities was compensated for by dividing $I(x,y)$ by a 2D parabolic function that approximately resembled the sum of squares of the coil sensitivity profile. More sophisticated methods to compensate for the coil sensitivity field exist, but this was found sufficient for the scope of this work.

3. Results

In Fig. 3A, the SNR maps for the two RF coils are shown, where the white dashed line corresponds to the 1D SNR profiles shown above. The eight-channel coil indicates a SNR variation by about a factor of 2 from the center to the edge of the phantom, and the 32-channel coil closer to a threefold difference, the latter being the coil used for successive experiments in this study. As the phantom had an 18-cm diameter, this SNR range is approximately what should be expected for an axial slice of the brain. In Fig. 3B, the sampling density, $D(x,y)$, of the iProp-FSE blades is shown for FOV ratios of 0.10, 0.15, 0.20 and 0.26, respectively. By multiplying the square root of the density map in Fig. 3B with the coil SNR map in Fig. 3A, the final SNR map, $S(x,y)$, is obtained (Fig. 3C). While for all phase-encoding FOVs the low coil SNR in the center is compensated for, an overall flatter SNR map is shown for a FOV ratio around or above 0.20. A too narrow FOV_{phase} (leftmost panel) clearly shows that the SNR is relatively high only at the center (from the averaging) and at the perimeter (due to the proximity of this region to the coil elements), while leaving a fairly large middle region with relatively low SNR. Notice also that the density maps do not include the aforementioned signal profile,$W(p)$. This is why the SNR pattern in Fig. 3C will have a softer appearance in practice.

Fig. 4 illustrates the iProp-FSE blade reconstruction. In Fig. 4A, a single blade is shown, where the signal drop-off at the edges along the phase-encoding direction is evident. Simply adding five iProp blades together without accounting for this signal profile prevents the blades from merging well together (Fig. 4B). When processing the five blade data according to Eq. (3), but without using the additional 1D Fermi filter, the resulting image becomes as in Fig. 4C. Already at this point, the blades are properly stitched together, except for some edge effects seen in low-signal areas. With the addition of the 1D Fermi filter in the reconstruction (Fig. 4D, red dotted line), the edge artifacts emanating from each blade are further suppressed (Fig. 4E), although in this example there are still too few blades to fully cover the entire FOV. With 10 blades in total, the final image appears as in Fig. 4F, being free from previous artifacts.

The results of the T2-blurring (effective resolution) measurements are summarized in Fig. 5. In Fig. 5A, the coronal spin-echo image is shown at the acquired FOV with the dashed orange box indicating the zoomed area shown in Fig. 5B and C. In the top-left corner of Fig. 5A, the four iProp-FSE blade widths that were used are sketched to scale. With the region of interest in the center of the FOV, all blades covered this area. In Fig. 5B, two extreme cases

are shown, the left being the Cartesian half-Fourier 320×320 SSFSE image with a sequence length of 900 ms (~10× the T2 of the brain), while the right is the same spin-echo data as in Fig. 5A not subject to any blurring in the phase-encoding direction. In Fig. 5C, the iProp-FSE data are shown for the same region vs. FOV ratio and rBW. The lowest T2 blurring occurs when the sequence length is the shortest, i.e., at ±63 kHz and a FOV ratio of 0.10, while being most prominent in the other end (bottom-left panel). The number in the panels is the sequence length relative to the shortest sequence (0.10 and ±63 kHz), a number that should be proportional to the amount of T2 blurring. As the blurring level increases continuously with these parameters, the maximum phase FOV and lowest rBW allowed may be somewhat subjective.

In Fig. 6, data from a healthy volunteer are shown using the same rBWs and FOV ratios as in Fig. 5. The orange annotations for each FOV ratio are the corresponding scan times, which differed due to the increased number of blades for narrow phase FOVs. On visual inspection by our neuroradiologist, the appreciated blurring is in concert with that of Fig. 5, where readout times longer than ~300 ms result in disturbing shearing of the image. In the comparison of the two most favorable images, FOV ratio=0.15 with rBW=±32 kHz and FOV ratio=0.2 with rBW=±62 kHz, the former was found to have slightly better GM/WM contrast. Each of the images in Fig. 6A was scanned twice, from which a pixel SNR map was calculated (not shown). From these maps, the mean value of a ROI over the center of the FOV was taken, where all blades overlap regardless of blade width (solid box in top-left panel, Fig. 6A). A ‘double ROI–was also put laterally to the first ROI (dashed boxes) from which the mean SNR was calculated. These two SNR values for each combination of FOV ratio and rBW are summarized in Fig. 6B. In concert with the more theoretical drawings in Fig. 3C, the SNR in the center is more similar to the ‘off-center–SNR when the blades are wider. However, for any blade width, the SNR is still 30–50% higher where the blades overlap compared to the off-center regions. Fig. 6C depicts SNR efficiency, η, for the dashed areas (being a better representative for the average brain SNR) for the single-slice and the multislice case (ignoring T1- and TR-dependent cross-talk issues).

In the single-slice limit, using a TR longer than ~3 s (for T2- w contrast purposes), there is a dramatic increase in SNR efficiency for wider blades. In this case, the most dramatic increase in SNR is for ±32 kHz, where the difference is over threefold between FOV ratios of 0.1 and 0.26. In this case, to gain the same SNR (cf. Fig. 6B) for a FOV of 0.1, about four times more blades are necessary, or in total 4×16 blades=64 blades, compared to the six for a FOV ratio of 0.26. However, by visual inspection, some of this SNR difference is attributed to the T2 blurring, which exaggerates this difference. Comparing to the relative SNR curves in Fig. 6B, it can be seen that the increase in SNR efficiency stems from both an actual increase in SNR and a decreased scan time.

In the multislice limit, the prescribed number of slices exceeds the minimum TR needed for T2-w contrast. This is why the sequence time has an impact on the SNR efficiency (assuming that TR is at a minimum for the selected number of slices). In this case, the shorter sequence time for narrower iProp blades compensates partly for the lost SNR efficiency at a narrower FOV_{phase} (Fig. 6C, green bars).

The cross-talk effect due to the tilted excitation slab is detailed in Fig. 7, with the left and right columns corresponding to an excitation tilt angle of 15° and 30°. At the top row, the single-slice case (no cross-talk) is shown for reference. For single-slice mode, the SNR is expected to be lower using a 15° flip angle, as the intersecting area between the excitation and refocusing pulses is diminished. However, the effect is reversed using a standard interleaving scheme (middle row) using a minimum TR for 32 adjacent slices, rendering the 30° tilt image very noisy due to the cross-slice saturation effects. For example, the basal ganglia are now quite difficult to outline adequately. With the proposed double-interleaved slice ordering scheme (bottom row), the situation is significantly improved. While the single-slice data are still superior in terms of SNR, the noise is significantly reduced, possibly with a slight advantage for the 30° tilt image.

For the remaining two figures presented in this work, the image resolution was increased to 448×448. In Fig. 8, single-slice volunteer data are shown, with the vendor's T2-w pulse sequences in the top row. Again, as an extreme case reference, Fig. 8A shows the SSFSE readout, which would correspond to an iProp-FSE scan using a FOV ratio of 1 and where all GM/WM contrast has been blurred out. The classical Cartesian FSE is shown in Fig. 8B, acquired in 2:00 min, but having minor motion artifacts in the frontal part of the brain, despite having been acquired on a cooperative volunteer (cf. yellow arrow in Fig. 8B). PROPELLER images acquired with 1.5 and 3 NEX (2:08 and 4:16 min) are shown in Fig. 8C and D. Compared to the FSE scan, PROPELLER images are not only free from motion artifacts, but also the contrast in the basal ganglia is somewhat improved with PROPELLER (even in the scan time-matched Fig. 8C and the use of a higher bandwidth).

In Fig. 8E–H, the iProp-FSE image reconstructed using 0:40–4:00 min worth of scan time is shown. In Fig. 8E, the SNR is clearly lower compared to that in Fig. 8B, but even here (after 40 s worth of scan time) the putamen and the internal capsule can be distinguished to an equal or better degree compared to FSE and PROPELLER. When comparing the scan time-matched PROPELLER (C) and iProp-FSE (G), iProp-FSE has less noise in the central part of the brain. Some colored noise is also apparent in (C). On the other hand, PROPELLER seems to have a slight advantage over iProp-FSE in the frontocortical white matter regions by a somewhat higher SNR.

Finally, reconstructions using 4–60 blades of a 60-blade iProp-FSE scan on a patient are outlined in Fig. 9. Here, the patient's ependymoma is visible already after the acquisition of blade data corresponding to four TRs (Fig. 9A), even before all parts of the brain have been acquired. After 10 blades (0:40 min), the SNR in the data is indeed further improved, making the images more appealing; however, the diagnostic confidence was not found to be significantly improved for this presented slice in Fig. 9D and E.

4. Discussion

We have presented a new pulse sequence, iProp-FSE, that may be a useful alternative for T2-w brain imaging using multichannel receive coils. With such coils, the SNR is vastly improved near the coil elements, while it drops rapidly toward the center of the coil. The local averaging of the central regions in iProp-FSE compensates for this effect. Despite the

fact that the SNR in each iProp-FSE blade due to its narrow FOV_{phase} is limited, the final SNR in the final image becomes sufficient. Depending on the width of the blades, the SNR due to averaging may vary to different extents between the inner circle (where the blades overlap) and the region just outside it. While we have overlapped the image blades in the center of the image, one may also consider overlapping them over a specific lesion to gain a high SNR over this area, while accepting higher noise levels in other parts of the anatomy.

We have chosen to tilt the excitation plane instead of the refocusing plane for three reasons: (i) to enable fewer RF pulses to hit neighboring slices, (ii) simplicity and (iii) to allow for some additional T1 relaxation in the excited out-of-slice area. One general side effect of a tilted excitation slab plane is the chemical shift from fat that is shifted perpendicular to this tilted plane –in a rotating fashion from one blade to the next. For brain imaging, with fat located mostly at the scalp, this would cause artifacts mostly near the perimeter of the brain, but, in this work, we chose to exclude this effect by using a leading fat-saturation pulse throughout all experiments.

Combing the iProp-blades into a final full-FOV image required the estimation of the 1D signal profile across the short axis of the blade. This was done using the average of all frequency-encoding lines and all blades on the acquired data themselves. To ensure zero weighting at the blade edges, a 1D Fermi filter was applied to both the image data and the weighting function. In this work, the blades were gridded separately and weighted in the final Cartesian space. In the future, a per-sample importance weighting option will be added to our gridding algorithm to enable all blades to be gridded at once –accounting for both variable sampling densities and blade intensities.

In this study, we have attempted to find adequate settings of the FOV_{phase} and receiver bandwidth, both of which control the sequence's readout time and hence the degree of T2 blurring. From both phantom and human brain data, we have found that a FOV ratio of 0.15 using ±32–62 kHz or up to 0.2 using (at least) ±62 kHz is a good trade-off between scan time, SNR and image sharpness for the resolutions used. For a fixed readout time, a larger FOV_{phase} at higher rBW is probably preferred over a smaller phase FOV and lower rBW, as the SNR ‘hotspot–created by the blade averaging in the center of the brain becomes wider.

For the comparison between FSE, PROPELLER and the fatsaturated iProp-FSE, the differences are, at first sight, small –even though fat saturation was used (to avoid aliasing fat) for iProp-FSE. FSE has some motion artifacts, typical even for data acquired on a cooperative healthy volunteer, while corresponding artifacts were absent in PROPELLER and iProp-FSE despite not performing any motion correction. In terms of delineating the deep brain matter, iProp-FSE was able to best outline the boundaries of putamen and deep gray matter structures, corresponding to the areas where many of the blades overlap. In the cortical brain matter, PROPELLER appeared slightly sharper than iProp-FSE for the acquisition parameters used. However, the difference is small. Moreover, as the PROPELLER data were reconstructed using propriety software, we did not possess full control of the data in this comparison.

The scan times reported in Fig. 8 show that iProp-FSE is by no means SNR starved, even in the peripheral areas being subject to fewer averages in iProp-FSE compared to FSE and PROPELLER. Moreover, it is interesting how few blades (and short scan time) are needed to achieve sufficient diagnostic quality without artifacts. Obviously, this is true in particular when the lesion of interest is in the center of the image FOV, such as in Fig. 9, and for many other brain stem diseases.

If there is severe out-of-plane motion, individual blades may need to be discarded (or down-weighted) for both PROPELLER and iProp-FSE. In the former, the undersampled *k*-space may introduce streaks in the data, while for iProp-FSE, wedges with missing data will ultimately occur. However, both PROPELLER and iProp-FSE are, in our experience, quite immune to undersampling effects (for example, see also Ref. [14]).

Motion correction between the iProp-FSE blades was not implemented or evaluated in this study. Nevertheless, it should be straightforward to do so using standard motion correction algorithms, with a sum-of-squares similarity measure to drive the registration process. Even if each image domain blade covers only a swath of the final FOV, there should be enough overlap between neighboring blades to drive the motion correction to the correct solution.

The biggest remaining issue for iProp-FSE is to make it efficient in the multislice mode. In this work, we have presented a double-interleaved slice ordering scheme to reduce the slice cross-talk. While this improved the SNR compared to standard interleaving, the single-slice scan was still better in terms of both SNR and tissue contrast. However, new zoom FOV techniques may be explored. The method of Dowell et al. [5] for contiguous slice zoom imaging, with two 180 pulses (for twice refocused DWI) being orthogonal to the intended scan plane, has by Ref. [15] shown to reduce the SNR and would be even less viable for iProp-FSE with its long echo train. However, a tilted version of the reduced FOV technique by Saritas et al. [6] was recently proposed by Finsterbusch [16], seemingly having neither the cross-talk limitation of our approach nor the slice count limitation of the approach of Saritas et al. [6]. However, the 2DRF excitation pulse will be longer, which increases the echo spacing if the CPMG condition is to be maintained.

5. Conclusions

A new motion robust T2-w pulse sequence, iProp-FSE, has been proposed and its characteristics explored. In terms of image quality and overall SNR efficiency, it is competitive compared to FSE and PROPELLER, and for the same scan time comes without colored noise or streaks from motion. In the deep brain matter regions, both SNR and image contrast appeared higher for iProp-FSE –already at shorter scan times. When a lesion of interest is localized, such as shown in this work on one patient, image domain blades can overlap this area very rapidly at sufficient SNR at the expense of lower SNR peripherally.

References

1. Hennig J, Nauerth A, Friedburg H. RARE imaging: a fast imaging method for clinical MR. Magn Reson Med. 1986; 3(6):823–33. [PubMed: 3821461]

2. Pipe JG. Motion correction with PROPELLER MRI: application to head motion and free-breathing cardiac imaging. Magn Reson Med. 1999; 42(5):963–9. [PubMed: 10542356]
3. Forbes KP, Pipe JG, Bird CR, Heiserman JE. PROPELLER MRI: clinical testing of a novel technique for quantification and compensation of head motion. J Magn Reson Imaging. 2001; 14(3): 215–22. [PubMed: 11536397]
4. Mansfield P, Ordidge RJ, Coxon R. Zonally magnified EPI in real time by NMR. J Phys E: Sci Instrum. 1988; 21:275–80.
5. Dowell NG, Jenkins TM, Ciccarelli O, Miller DH, Wheeler-Kingshott CA. Contiguous-slice zonally oblique multislice (CO-ZOOM) diffusion tensor imaging: examples of in vivo spinal cord and optic nerve applications. J Magn Reson Imaging. 2009; 29(2):454–60. [PubMed: 19161202]
6. Saritas EU, Cunningham CH, Lee JH, Han ET, Nishimura DG. DWI of the spinal cord with reduced FOV single-shot EPI. Magn Reson Med. 2009; 60(2):468–73. [PubMed: 18666126]
7. Deng J, Larson AC. Multishot targeted PROPELLER magnetic resonance imaging: description of the technique and initial applications. Invest Radiol. 2009; 44(8):454–62. [PubMed: 19465860]
8. Norris DG. Ultrafast low-angle RARE: U-FLARE. Magn Reson Med. 1991; 17(2):539–42. [PubMed: 2062221]
9. Norris DG, Bornert P, Reese T, Leibfritz D. On the application of ultra-fast RARE experiments. Magn Reson Med. 1992; 27(1):142–64. [PubMed: 1435200]
10. Pipe JG, Zwart N. Turboprop: improved PROPELLER imaging. Magn Reson Med. 2006; 55(2): 380–5. [PubMed: 16402378]
11. Skare S, Newbould RD, Clayton DB, Bammer R. Propeller EPI in the other direction. Magn Reson Med. 2006; 55(6):1298–307. [PubMed: 16676335]
12. Haacke EM, Lindskog ED, Lin W. A fast, iterative, partial-Fourier technique capable of local phase recovery. J Magn Reson. 1991; 92(1):126–45.
13. Liang ZP. Constrained reconstruction methods in MR imaging. Rev Magn Reson Med. 1992; 4:67–185. [review].
14. Arfanakis K, Tamhane AA, Pipe JG, Anastasio MA. *k*-Space undersampling in PROPELLER imaging. Magn Reson Med. 2005; 53(3):675–83. [PubMed: 15723398]
15. Jeong EK, Kim SE, Guo J, Kholmovski EG, Parker DL. High-resolution DTI with 2D interleaved multislice reduced FOV single-shot diffusion-weighted EPI (2D ssrFOV- DWEPI). Magn Reson Med. 2005; 54(6):1575–9. [PubMed: 16254946]
16. Finsterbusch, J. Diffusion-weighted inner-field-of-view EPI using 2D-selective RF excitations with a tilted excitation plane. Proceedings of the 19th Annual Meeting of ISMRM; Montreal, Canada. 2011. p. 174

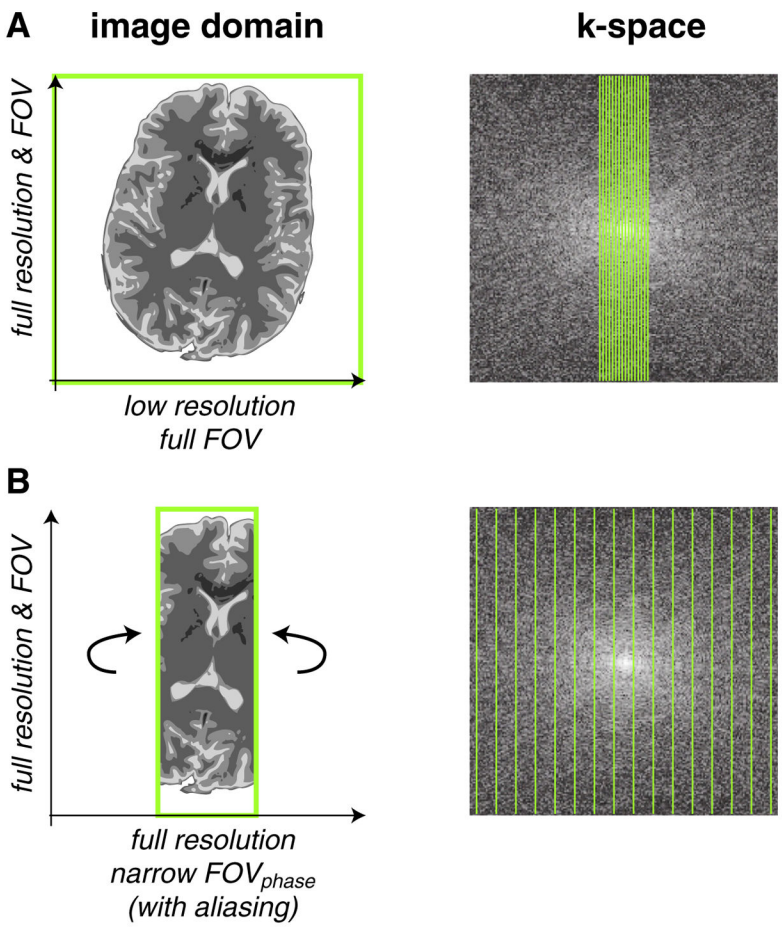

Fig. 1.

Illustration of the *k*-space propeller (A) and the image space propeller (B) trajectory (this work). In (A), the *k*-space blade corresponds to a full FOV image with low resolution along the phase-encoding direction. In (B), the image domain blade has the same image resolution as the final image, but with a reduced phase-encoding FOV, leading to aliasing if not accounted for.

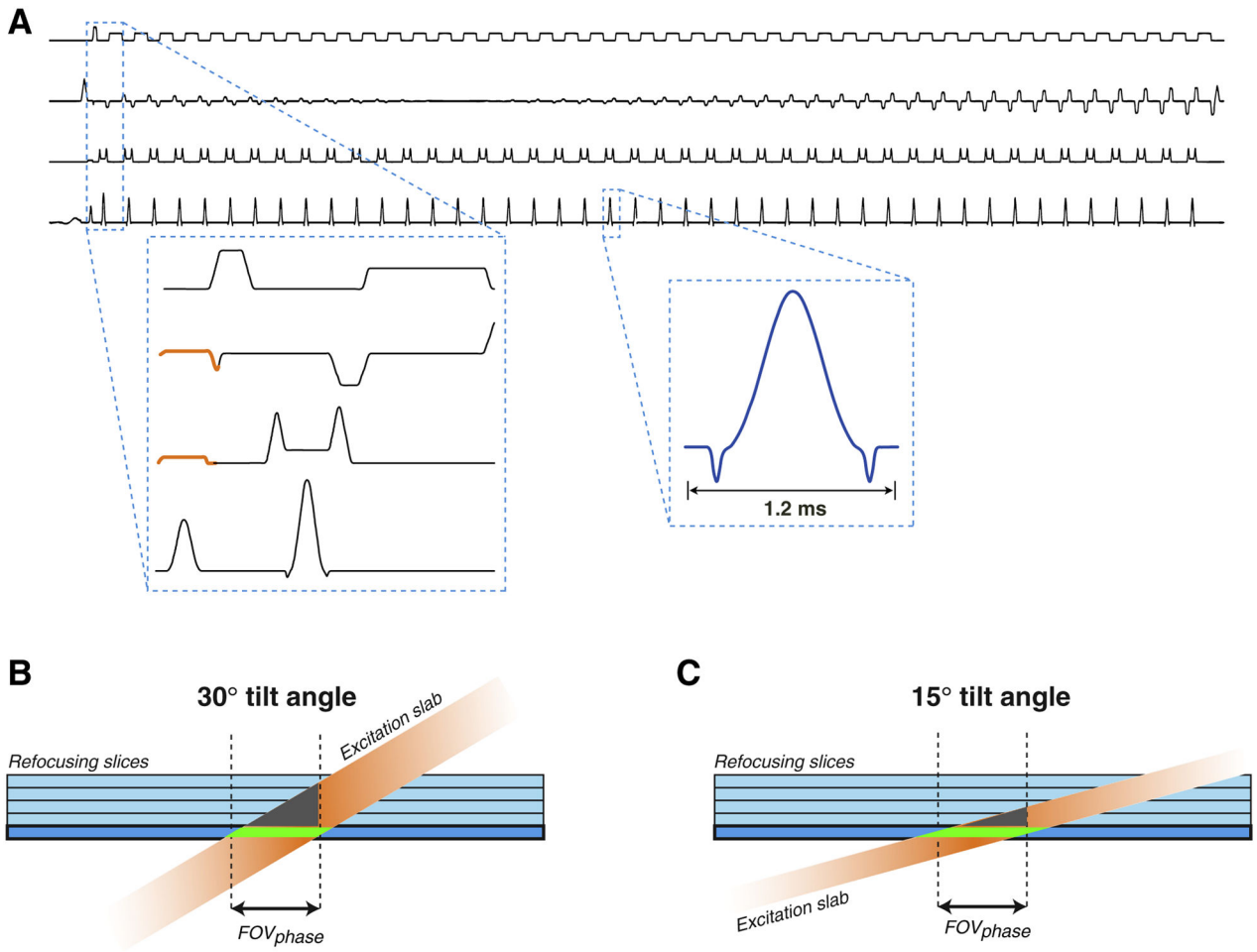

Fig. 2.

(A) The iProp-FSE pulse sequence. Insets show the added excitation gradient that rotates the excitation slice into the slice/phase plane as shown in (B) and (C). The green areas in (B) and (C) show the intersecting area of the excitation and refocusing pulses from where the spin-echo signal originates. The gray wedges show the regions where the excitation slab (unfortunately) saturates spins to be excited in subsequent excitations.

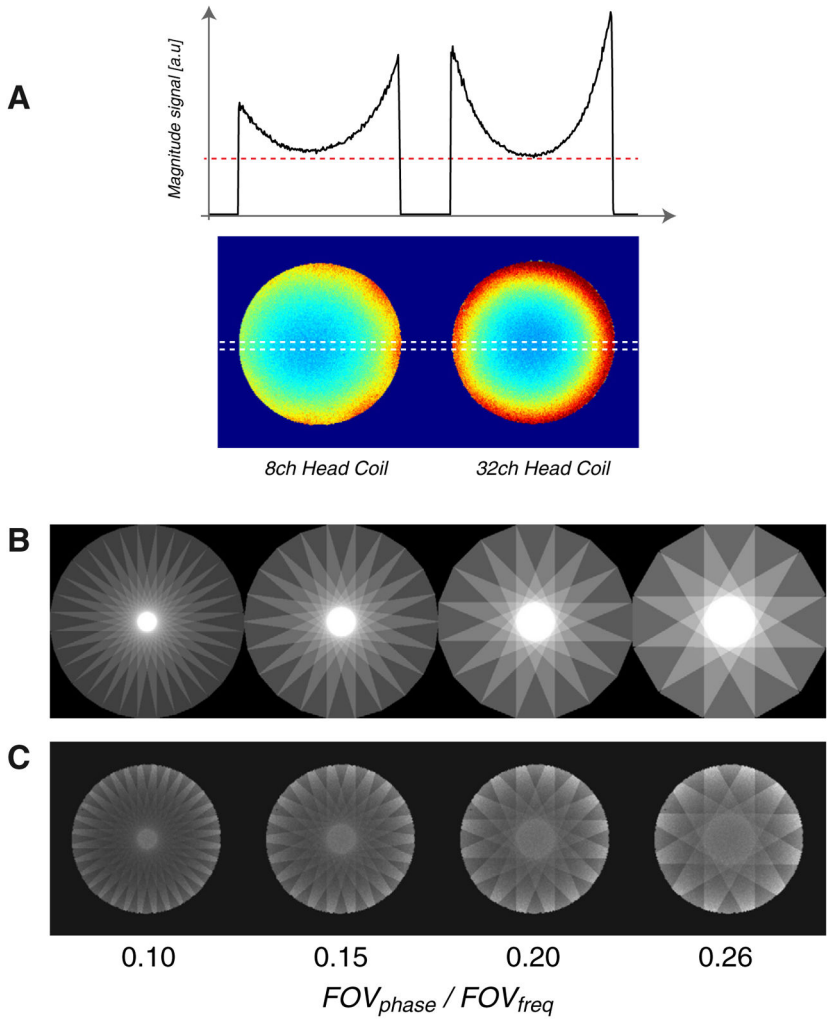

Fig. 3.

(A) Axial SNR maps of two multichannel head coils. The right one was used in this work. (B) The spatially varying averaging ('NEX') map due to the overlapping iProp-FSE blades shown for the FOV ratios used in this study. (C) Final SNR map, accounting for both the spatially varying SNR due to the receiver coils and due to the blade averaging. Overall, this evens out the SNR variation shown in (A).

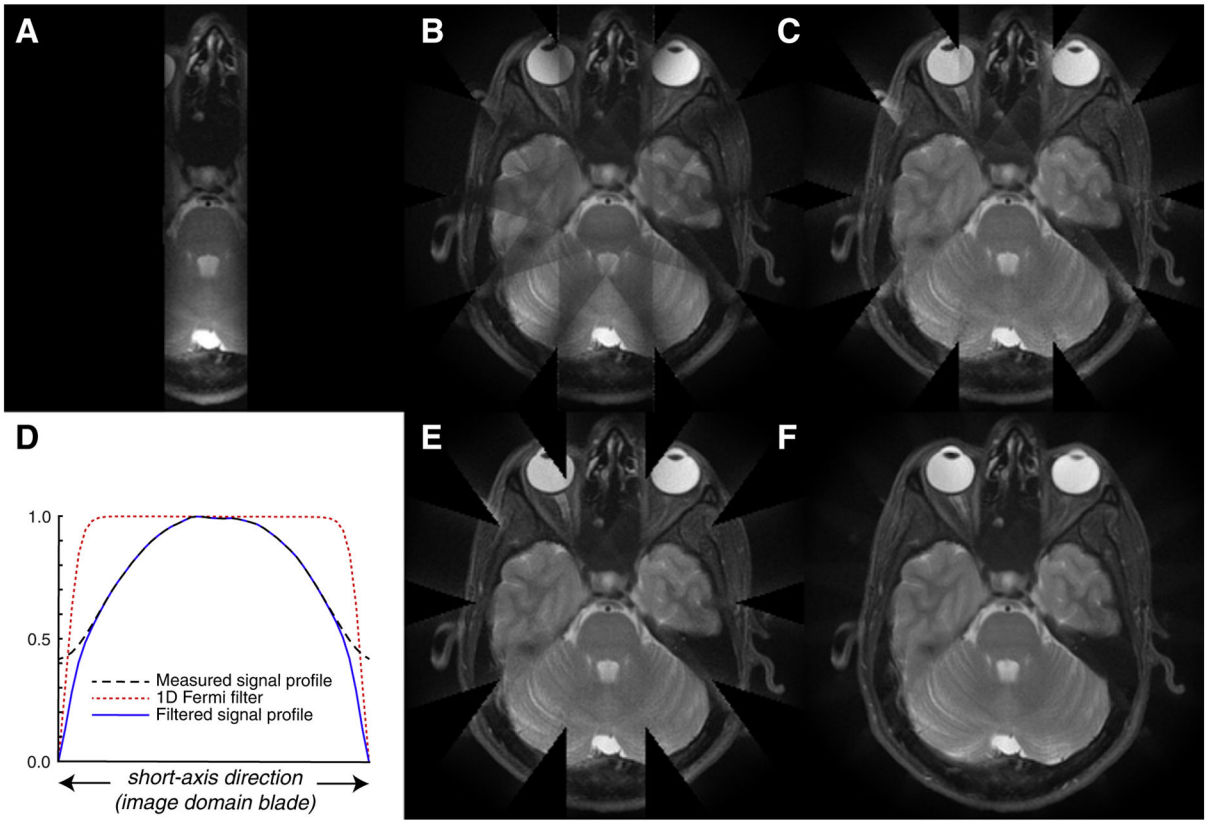

Fig. 4.

(A) One iProp-FSE blade. (B) The full FOV image, obtained by plain averaging five iProp-FSE blades together. (C) The same data using the importance weighting filter due to the measured signal response in the phase-encoding direction of the blades (black dashed line, D). (E) Same as (C), but using an additional 1D Fermi filter (red dotted line, D) to force down the noisy (and partially wrapped) signal at the edges of the blades (blue solid line, D). (F) Same as (E), but with 10 iProp-FSE blades.

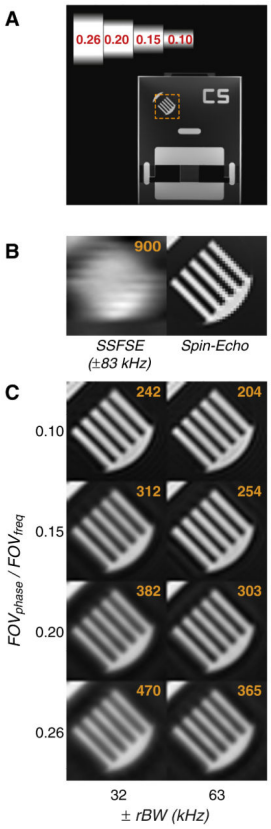

Fig. 5.

(A) Overview of the full FOV acquired in this experiment, with the dashed box outlining the area shown in (B) and (C). In the top-left corner in (A), the blade widths used are shown to scale. (B) Reference images. Left: SSFSE with highest available receiver bandwidth, yet resulting in a 900-ms-long readout and hence severe T2 blurring. Right: The classical spin-echo image (left half interpolated, right half showing the native pixels used). (C) iProp-FSE reconstructions at FOV ratios of 0.1–0.26 and receiver bandwidths of ±32 and ±62 kHz. The number (orange) in the right corner of each image represents the readout time in milliseconds. Blurring starts to become apparent over ~300 ms.

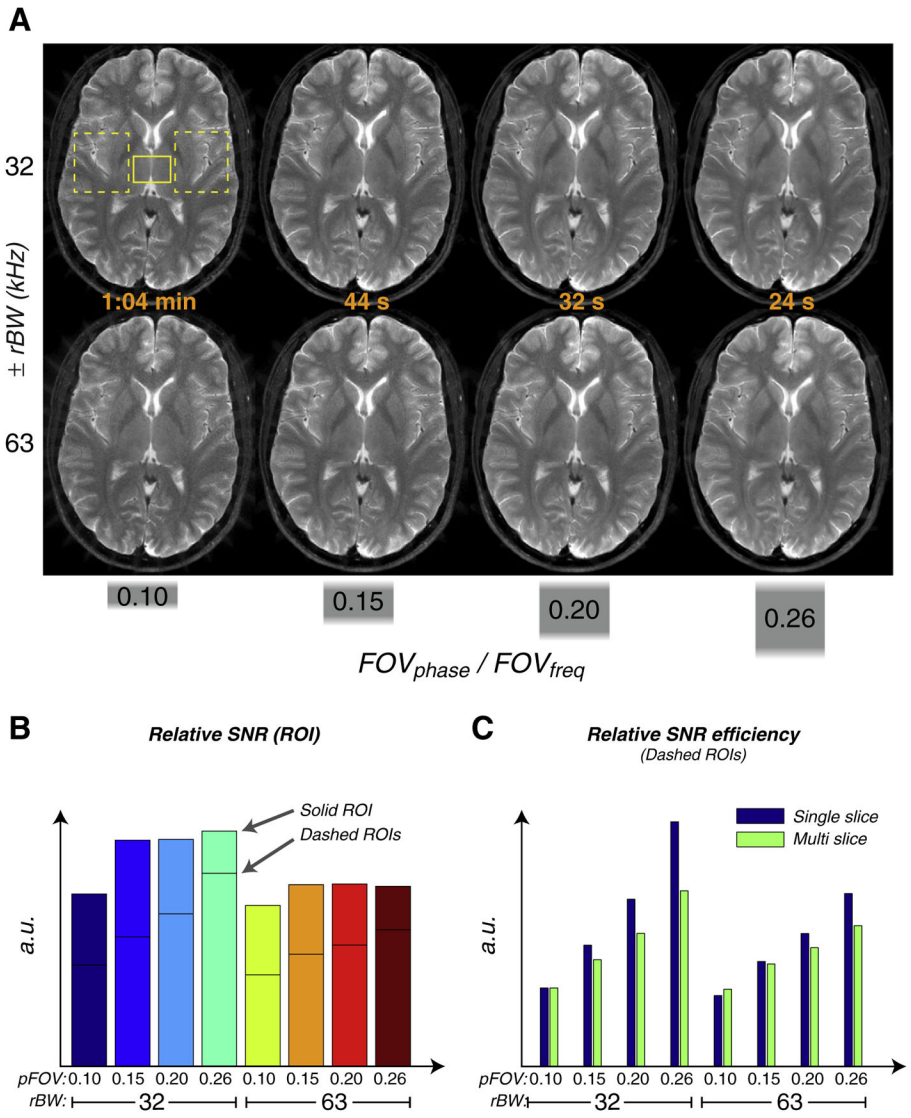

Fig. 6.

Volunteer data. (A) Same layout as in Fig. 5, showing the trade-off between scan time, noise and T2 blurring. A FOV ratio of 0.15 and a rBW of ±32 kHz were found to be the most favorable image, in terms of image contrast just slightly better than the 0.20/±63 kHz image. (B) Bar graphs showing the relative SNR between the eight images, using data from the two ROIs (note the dual height bars). These SNR measurements are due to a mix of true SNR and the smearing effect of the T2 blurring. (C) The SNR efficiency (cf. Eqs. (1) and (2)) shown for both the single-slice and multislice scenario. While the SNR efficiency is outstanding for 0.26/±32 kHz due to the few blades needed, low bandwidth and wide FOV_{phase}, the T2 blurring becomes prohibitively large at this point. The variation with FOV_{phase} becomes less for the multislice scenario since the sequence's readout length is accounted for.

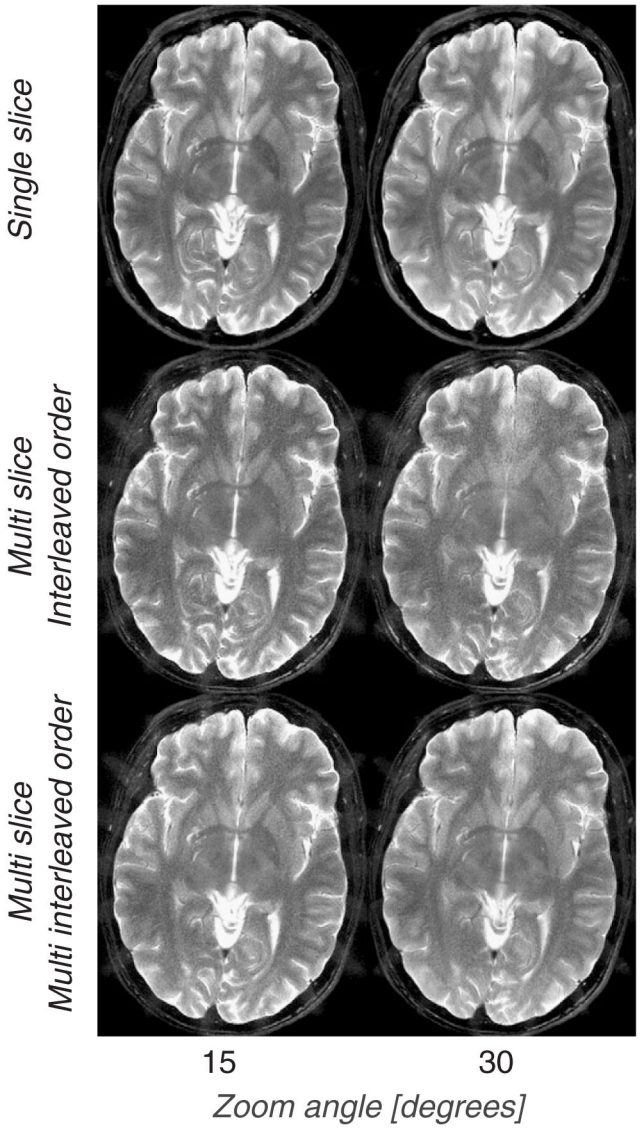

Fig. 7.

Top row: Single-slice at tilt angles of 15° and 30°, respectively. In the absence of slice cross-talk, the larger effective slice thickness for higher flip angles at the blade edges (green area, Fig. 2B and C) results in an image with higher SNR. Middle row: Standard interleaved multislice imaging (32 slices) using the same acquisition parameters as for the top row, the 15° tilt angle image, where the neighboring slices have been less saturated (gray areas, Fig. 2B and C), has both higher SNR and better tissue contrast compared to the 30° image. Bottom row: With our proposed interleaving scheme, these multislice effects are much more benign, with less noise in the 30° case, albeit not quite as high ‘SNR as for ‘single-slice ones.

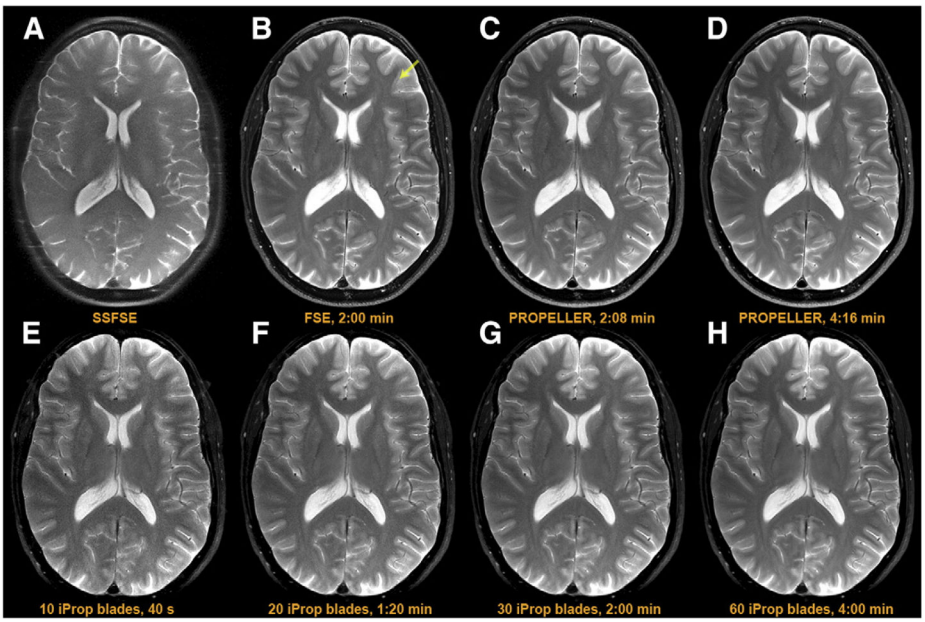

Fig. 8.

Single-slice 448×448 resolution T2-w data, volunteer. (A) SSFSE. (B) Fast spin echo. (C) PROPELLER, 1.5 NEX. (D) PROPELLER, 3 NEX. (E–H) iProp-FSE reconstructions of a 60-blade scan using (E) 10, (F) 20, (G) 30 and (H) all 60 blades. For the deep brain matter, already in (E) the tissue contrast was found to be better than the 2-min-long FSE and PROPELLER scans (B and C). The minor streaks for FSE due to motion are absent in both PROPELLER and iProp-FSE. Comparing the 2/4 min scans, (C/D) PROPELLER and (G/H) iProp-FSE, the putamen and internal capsule are better outlined for iProp-FSE with less colored noise, while the SNR in the frontocortical structures has somewhat lower noise for PROPELLER.

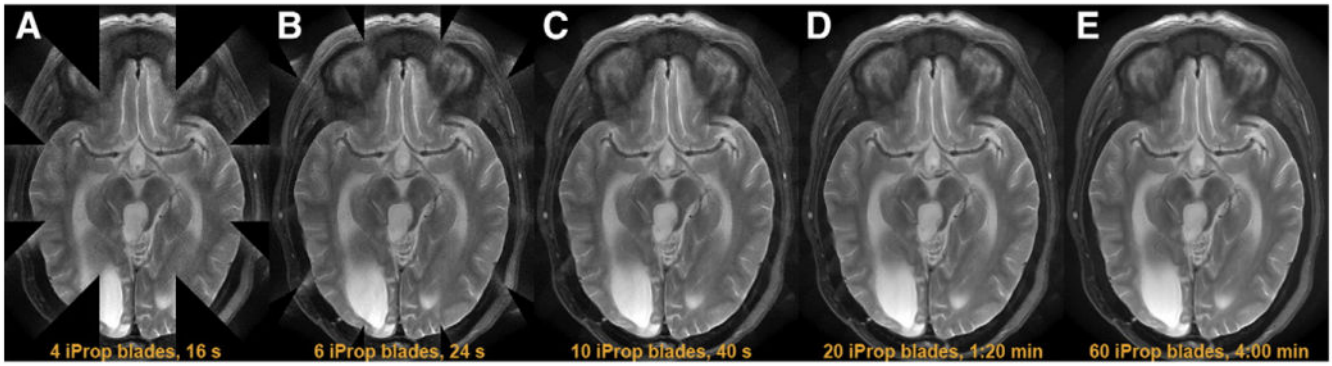

Fig. 9.

Patient with an ependymoma, located in the center of the image FOV, acquired with 60 iProp-FSE blades in 4 min. Already after four TRs (16 s), the lesion is outlined with sufficient diagnostic image quality, yet the image FOV not being fully acquired.